

Electronic Supplementary Information (ESI)

for *CrystEngComm*

Modulating the Structural Topologies from Star-shape to Cross-shape for the Co-Dy Heterometallic Complexes with Slow Magnetic Relaxation Behavior

Hui-Sheng Wang,^{*a} Chun-Fang Yu,^a Si-Qi Ye,^a Yong Chen,^a Xueru Liu,^{*b} Yanfang Wu,^{*c} Pengfei Zhou^a and Yi-Quan Zhang^d

^a School of Chemistry and Environmental Engineering, Key Laboratory of Green Chemical Process of Ministry of Education, Key Laboratory of Novel Reactor and Green Chemical Technology of Hubei Province, Wuhan Institute of Technology, Wuhan 430074, P. R. China.

^b College of Chemistry and Materials Science, Northwest University, Xi'an 710127, P. R. China.

^c School of Energy and Mechanical Engineering, Jiangxi University of Science and Technology, Nanchang 330013, P. R. China.

^d School of Physical Science and Technology, Nanjing Normal University, Nanjing 210023, P. R. China.

Corresponding Author

*Email: wangch198201@163.com (H.S. Wang).

*Email: lxueru@nwu.edu.cn (Xueru Liu).

*Email: wuyanfang1208@163.com (Y. Wu).

Table S1. Crystallographic Data for compounds **1** and **2**.

Compounds	1	2
Formula ^a	C ₄₈ H ₅₅ Co ₂ Dy ₂ N ₁₂ O _{25.50}	C ₁₀₈ H ₁₄₁ Co ₇ DyN ₁₅ O ₄₃
Formula weight ^a	1650.90	2912.36
Crystal colour	brown	dark brown
Crystal size/mm	0.26 × 0.20 × 0.06	0.27 × 0.24 × 0.17
Crystal system	triclinic	monoclinic
Space group	<i>P</i> $\bar{1}$	<i>P</i> 2 ₁ / <i>n</i>
<i>a</i> (Å)	11.9878(17)	23.2569(10)
<i>b</i> (Å)	13.4630(19)	19.2410(8)
<i>c</i> (Å)	19.444(3)	28.2143(14)
α (°)	103.072(2)	90
β (°)	97.912(2)	101.344(2)
γ (°)	100.201(2)	90
Unit cell volume (Å ³)	2956.4(7)	12378.9(10)
Temperature (K)	296(2)	173(2)
<i>Z</i>	2	4
Wavelength (Å)	0.71073	0.71073
μ (Mo <i>K</i> α) [mm ⁻¹]	3.144	1.599
<i>D</i> _c (g cm ⁻³)	1.855	1.563
θ range (°)	2.19- 20.58	2.9455-25.3954
Index ranges	-14 ≤ <i>h</i> ≤ 13 -15 ≤ <i>k</i> ≤ 15 -23 ≤ <i>l</i> ≤ 23	-27 ≤ <i>h</i> ≤ 25 -22 ≤ <i>k</i> ≤ 21 -33 ≤ <i>l</i> ≤ 33
<i>F</i> (000)	1634	5972
Reflections collected	27817	67104
Unique reflections [<i>R</i> _{int}]	10291 [0.0645]	21537 [0.0613]
Reflections with <i>I</i> > 2σ(<i>I</i>)	7258	15343
Final <i>R</i> indices (<i>I</i> > 2σ(<i>I</i>)) _{b,c}	<i>R</i> ₁ = 0.0457, <i>wR</i> ₂ = 0.0842	<i>R</i> ₁ = 0.0648, <i>wR</i> ₂ = 0.1294
Final <i>R</i> indices (all data)	<i>R</i> ₁ = 0.0736, <i>wR</i> ₂ = 0.0895	<i>R</i> ₁ = 0.1038, <i>wR</i> ₂ = 0.1420
<i>S</i> (all data)	1.192	1.084
(Δρ) _{max,min} /e Å ⁻³	1.487 and -1.086	1.957 and -1.325

^a The formula and the formula weights include the H₂O and MeCN solvent molecules which were free.

^b $R_1 = \Sigma(|F_o| - |F_c|)/\Sigma|F_o|$. ^c $wR_2 = [\Sigma[w(F_o^2 - F_c^2)^2]/\Sigma[w(F_o^2)^2]]^{1/2}$, $w = 1/[\sigma^2(F_o^2) + [(ap)^2 + bp]$, where $p = [\max(F_o^2, 0) + 2F_c^2]/3$.

Table S2. Selected bond lengths (Å) and angles (°) for **1**.

Selected bond lengths for 1					
Co1-O1	1.884(4)	Co2-O9	1.922(4)	Dy2-O10	2.247(4)
Co1-O3	1.892(4)	Co2-O7	1.963(4)	Dy2-O2	2.270(4)
Co1-N2	1.921(6)	Dy1-O9	2.287(4)	Dy2-O23	2.371(4)
Co1-N1	1.936(5)	Dy1-O10	2.296(4)	Dy2-O21	2.439(5)
Co1-N3	1.930(5)	Dy1-O1	2.324(4)	Dy2-O17	2.455(6)
Co1-N4	1.948(6)	Dy1-O7	2.367(4)	Dy2-O18	2.456(6)
Co2-O5	1.878(4)	Dy1-O6	2.425(4)	Dy2-O15	2.491(6)
Co2-N5	1.886(6)	Dy1-O2	2.434(4)	Dy2-O20	2.512(5)
Co2-O8	1.885(5)	Dy1-O11	2.454(5)	Dy2-O14	2.537(5)
Co2-N6	1.904(6)	Dy1-O12	2.430(5)		

Selected bond angles for 1					
O1-Co1-O3	93.71(18)	O10-Dy1-O1	122.56(14)	O2-Dy2-O15	149.6(2)
O1-Co1-N2	83.5(2)	O9-Dy1-O7	70.18(15)	O23-Dy2-O15	96.6(2)
O3-Co1-N2	91.2(2)	O10-Dy1-O7	79.85(15)	O21-Dy2-O15	70.0(2)
O1-Co1-N3	175.7(2)	O1-Dy1-O7	119.27(15)	O17-Dy2-O15	67.8(2)
O3-Co1-N3	83.5(2)	O9-Dy1-O6	89.92(15)	O18-Dy2-O15	67.5(2)
N2-Co1-N3	93.3(2)	O10-Dy1-O6	155.27(16)	O10-Dy2-O20	80.15(16)
O1-Co1-N1	81.3(2)	O1-Dy1-O6	70.63(14)	O2-Dy2-O20	79.75(16)
O3-Co1-N1	175.0(2)	O7-Dy1-O6	75.43(15)	O23-Dy2-O20	155.48(16)
O5-Co2-O9	91.28(19)	O9-Dy1-O12	88.38(16)	O21-Dy2-O20	51.65(17)
N5-Co2-O9	93.0(2)	O10-Dy1-O12	77.76(17)	O17-Dy2-O20	120.3(2)
O8-Co2-O9	178.18(19)	O1-Dy1-O12	88.79(16)	O18-Dy2-O20	71.3(2)
N6-Co2-O9	84.2(2)	O7-Dy1-O12	150.77(16)	O15-Dy2-O20	107.4(2)
O5-Co2-O7	177.75(19)	O6-Dy1-O12	125.70(17)	O10-Dy2-O14	87.9(2)
N5-Co2-O7	83.4(2)	O9-Dy1-O2	149.27(15)	O2-Dy2-O14	150.21(18)
O8-Co2-O7	91.23(19)	O10-Dy1-O2	68.71(15)	O23-Dy2-O14	71.69(17)
N6-Co2-O7	95.5(2)	O1-Dy1-O2	57.21(14)	O21-Dy2-O14	68.57(19)
O9-Co2-O7	87.08(18)	O7-Dy1-O2	93.76(14)	O17-Dy2-O14	102.8(2)
O9-Dy1-O10	82.43(15)	O6-Dy1-O2	111.84(15)	O18-Dy2-O14	118.5(2)
O9-Dy1-O1	153.52(15)	O10-Dy2-O15	137.3(2)	O20-Dy2-O14	119.63(19)

Table S3. Selected bond lengths (Å) and angles (°) in **2**.

Selected bond lengths in 2					
Co1-O1	1.900(5)	Co3-O9	1.913(5)	Co6-O23	1.903(5)
Co1-O4	1.910(5)	Co3-O11	1.913(5)	Co6-N8	1.910(6)
Co1-N1	1.911(6)	Co4-O13	1.884(5)	Co6-N7	1.912(6)
Co1-O5	1.914(5)	Co4-N5	1.891(6)	Co6-O19	1.930(5)
Co1-N2	1.917(6)	Co4-N6	1.896(6)	Co7-O25	1.895(4)
Co1-O2	1.925(4)	Co4-O15	1.898(4)	Co7-N9	1.915(6)
Co2-O5	2.056(4)	Co4-O17	1.912(5)	Co7-N10	1.917(6)
Co2-O14	2.060(4)	Co4-O16	1.933(5)	Co7-N10 ⁱ	1.918(6)
Co2-O3	2.093(4)	Co5-O12	2.054(5)	Dy1-O8	2.241(4)
Co2-O6	2.106(5)	Co5-O20	2.060(5)	Dy1-O18	2.250(4)
Co2-O8	2.112(4)	Co5-O24	2.101(4)	Dy1-O14	2.252(4)
Co2-O2	2.142(4)	Co5-O21	2.110(5)	Dy1-O12	2.267(4)
Co3-O7	1.890(5)	Co5-O18	2.113(4)	Dy1-O15	2.468(4)
Co3-N3	1.897(6)	Co5-O23	2.129(5)	Dy1-O11	2.498(4)
Co3-O10	1.897(5)	Co6-O22	1.888(5)	Dy1-O9	2.528(5)
Co3-N4	1.912(6)	Co6-O20	1.888(5)	Dy1-O17	2.548(5)
Selected bond angles in 2					
O1-Co1-O4	91.6(2)	N5-Co4-O16	87.2(2)	O25-Co7-N10	83.6(2)
O1-Co1-N1	94.9(2)	N6-Co4-O16	94.7(2)	N9-Co7-N10	88.6(3)
O4-Co1-N1	86.5(2)	O15-Co4-O16	89.7(2)	O25-Co7-N9	83.6(2)
O1-Co1-O5	89.6(2)	O17-Co4-O16	175.4(2)	O8-Dy1-O18	111.69(15)
O14-Co2-O6	89.28(17)	O24 Co5 O23	89.43(17)	O8-Dy1-O14	76.04(14)
O3-Co2-O6	178.44(18)	O21 Co5 O23	90.42(18)	O18-Dy1-O14	150.87(16)
O5-Co2-O8	98.03(17)	O18 Co5 O23	175.74(18)	O14-Dy1-O12	111.60(15)
O14-Co2-O8	83.10(16)	O12 Co5 Co6	139.41(12)	O8-Dy1-O15	134.89(15)
O10-Co3-O9	91.8(2)	O22-Co6-O23	177.9(2)	O12-Dy1-O15	73.98(15)
N4-Co3-O9	93.4(2)	O20-Co6-O23	88.0(2)	O8-Dy1-O11	78.05(15)
O7-Co3-O11	90.6(2)	O22-Co6-N8	94.5(3)	O11-Dy1-O9	62.45(15)
N3-Co3-O11	94.3(2)	O20-Co6-N8	89.1(2)	O8-Dy1-O17	76.16(15)

Table S4. Bond valence sum (BVS) calculations for determining of the protonation levels of the O atoms in **1** and **2**.

Atoms in 1	BVS values of 1	Atoms in 1	BVS values of in 1
O1	1.86	O2	1.85
O3	1.51	O4	2.21
O5	1.75	O6	1.24
O7	1.71	O8	1.76
O9	1.87	O10	1.92
O11	1.85	O12	1.82
O13	1.78	O14	1.98
O15	1.84	O16	1.50
O17	1.94	O18	1.84
O19	1.76	O20	1.78
O21	1.83	O22	1.71
O23	1.31		

Atoms in 2	BVS values of 2	Atoms in 2	BVS values of 2
O1	1.70	O15	1.70
O2	1.68	O16	1.74
O3	1.25	O17	1.60
O4	1.76	O18	1.87
O5	1.74	O19	1.60
O6	1.27	O20	1.75
O7	1.71	O21	1.21
O8	1.87	O22	1.77
O9	1.65	O23	1.75
O10	1.70	O24	1.23
O11	1.72	O25	1.44
O12	1.87	O26	1.02
O13	1.73	O27	1.45
O14	1.90	O28	1.09

The values of BVS calculations for O atoms in the ~ 1.8 – 2.0 , ~ 1.0 – 1.2 , and ~ 0.2 – 0.4 ranges are indicative of non-, single- and double-protonation, respectively. The O atoms with one H atoms were labeled by red.

Table S5. Bond valence sum (BVS) calculations for determining of the oxidation of the Co atoms in **1** and **2**.

Co atoms in complex 1	Co (II)	Co (III)
Co (1)	3.05	<u>3.46</u>
Co (2)	3.19	<u>3.21</u>
Co atoms in complex 2	Co (II)	Co (III)
Co (1)	3.186	<u>3.185</u>
Co (2)	<u>2.026</u>	1.747
Co (3)	3.266	<u>3.266</u>
Co (4)	3.277	<u>3.289</u>
Co (5)	<u>2.027</u>	1.747
Co (6)	3.256	<u>3.250</u>

Table S6. The possible geometries of oct-coordination metal centers and Deviation parameters from each ideal polyhedron for Dy1 in **1**.

Point group	Geometry	Polyhedron	Deviation of Dy1
D_{8h}	OP-8	Octagon	33.913
C_{7v}	HPY-8	Heptagonal pyramid	22.890
D_{6h}	HBPY-8	Hexagonal bipyramid	15.571
O_h	CU-8	Cube	10.011
D_{4d}	SAP-8	Square antiprism	4.655
D_{2d}	TDD-8	Triangular dodecahedron	3.061
D_{2d}	JGBF-8	Johnson - Gyrobifastigium (J26)	13.709
D_{3h}	JETBPY-8	Johnson - Elongated triangular bipyramid (J14)	25.838
C_{2v}	JBTP-8	Johnson - Biaugmented trigonal prism (J50)	4.207
C_{2v}	BTPR-8	Biaugmented trigonal prism	3.350
D_{2d}	JSD-8	Snub disphenoid (J84)	6.163
T_d	TT-8	Triakis tetrahedron	10.735
D_{3h}	ETBPY-8	Elongated trigonal bipyramid	21.001

Note: The coordination geometry of Dy1 was labeled by red.

Table S7. The possible geometries of nona-coordination metal centers and Deviation parameters from each ideal polyhedron for Dy2 in **1**.

Point group	Geometry	Polyhedron	Deviation of Dy2
D_{9h}	EP-9	Enneagon	36.050
C_{8v}	OPY-9	Octagonal pyramid	24.070
D_{7h}	HBPY-9	Heptagonal bipyramid	18.705
C_{3v}	JTC-9	trivacant cuboctahedron	14.822
C_{4v}	JCCU-9	Capped cube (Elongated square pyramid, J8)	9.952
C_{4v}	CCU-9	Capped cube	8.482
C_{4v}	JCSAPR-9	Capped sq. antiprism (Gyroelongated square pyramid J10)	3.530
C_{4v}	CSAPR-9	Capped square antiprism	2.569
D_{3h}	JTCTPR-9	Tricapped trigonal prism (J51)	4.566
D_{3h}	TCTPR-9	Tricapped trigonal prism	3.144
C_{3v}	JTDIC-9	Tridiminished icosahedron (J63)	13.145
C_{2v}	HH-9	Hula-hoop	10.366
C_s	MFF-9	Muffin	1.971

Note: The coordination geometry of Dy2 was labeled by red.

Table S8. The possible geometries of oct-coordination metal centers and Deviation parameters from each ideal polyhedron for Dy1 in **2**.

Point group	Geometry	Polyhedron	Deviation of Dy1
D_{8h}	OP-8	Octagon	24.859
C_{7v}	HPY-8	Heptagonal pyramid	25.533
D_{6h}	HBPY-8	Hexagonal bipyramid	14.615
O_h	CU-8	Cube	9.488
D_{4d}	SAP-8	Square antiprism	1.405
D_{2d}	TDD-8	Triangular dodecahedron	2.878
D_{2d}	JGBF-8	Johnson - Gyrobifastigium (J26)	11.456
D_{3h}	JETBPY-8	Johnson - Elongated triangular bipyramid (J14)	26.558
C_{2v}	JBTP-8	Johnson - Biaugmented trigonal prism (J50)	1.853
C_{2v}	BTPR-8	Biaugmented trigonal prism	2.103
D_{2d}	JSD-8	Snub disphenoid (J84)	2.590
T_d	TT-8	Triakis tetrahedron	10.229
D_{3h}	ETBPY-8	Elongated trigonal bipyramid	23.455

Note: The coordination geometry of Dy1 was labeled by red.

Table S9. The details of the parameters of square antiprism (SAP) of Dy^{III} in **2**.

Skew angle (ϕ , °)		Skew angle (ϕ , °)	
$\phi_1 = 35.61(1)$	$\phi_2 = 51.95(1)$	$\phi_3 = 39.30(1)$	$\phi_4 = 53.15(2)$
Mean value of $\phi = 45.00(1)$			
Parameter γ (°)		Magic angles α (°)	
$\gamma(\text{O15-Dy1-O11}) = 128.20$	$\gamma(\text{O12-Dy1-O14}) = 111.60$	$\alpha(\text{O15-O11}) = 64.10$	$\alpha(\text{O12-O14}) = 55.80$
$\gamma(\text{O18-Dy1-O8}) = 111.68$	$\gamma(\text{O9-Dy1-O17}) = 133.01$	$\alpha(\text{O18-O8}) = 55.84$	$\alpha(\text{O9-O17}) = 66.51$
Mean value of $\gamma = 121.12$		Mean value of $\alpha = 60.56$	
Values of d_{in} (Å)		Values of $d_{\text{pp}}(\text{A-B})$ (Å)	
$d_{\text{in}}(\text{O14-O15}) = 2.98(6)$	$d_{\text{in}}(\text{O15-O12}) = 2.85(5)$	$d_{\text{pp}}(\text{O11-B}) = 2.24(1)$	$d_{\text{pp}}(\text{O12-B}) = 2.41(8)$
$d_{\text{in}}(\text{O12-O11}) = 2.98(6)$	$d_{\text{in}}(\text{O11-O14}) = 2.86(5)$	$d_{\text{pp}}(\text{O15-B}) = 2.22(5)$	$d_{\text{pp}}(\text{O14-B}) = 2.41(8)$
$d_{\text{in}}(\text{O18-O17}) = 3.03(6)$	$d_{\text{in}}(\text{O17-O8}) = 2.97(6)$	$d_{\text{pp}}(\text{O9-B}) = 2.21(0)$	$d_{\text{pp}}(\text{O8-B}) = 2.45(5)$
$d_{\text{in}}(\text{O8-O9}) = 3.01(6)$	$d_{\text{in}}(\text{O9-O18}) = 2.95(6)$	$d_{\text{pp}}(\text{O17-B}) = 2.17(9)$	$d_{\text{pp}}(\text{O18-B}) = 2.43(2)$
Mean value of $d_{\text{in}} = 2.95$		$d_{\text{pp}}^{\#}(\text{A-B}) = 2.32$	$d_{\text{pp}}^* = 2.31$
Dihedral angle (θ , °)		σ_{ϕ}^2 and σ_{α}^2	
$\theta = 0.40$		$\sigma_{\phi}^2 = 58.85$, $\sigma_{\alpha}^2 = 57.17$	

Note: The means of the parameters: ϕ is skew angle between the diagonals of two square faces, α is the magic angles between the pseudo S_8 axis and the directions of the Dy-O bonds, d_{in} is the distances between the coordination atoms in each plane, d_{pp} is the interplanar distances between two planes and θ is the angle between two square planes. $\phi_1 = \phi(\text{O12O14}[\text{Dy1}]\text{O18O8})$, $\phi_2 = \phi(\text{O18O8}[\text{Dy1}]\text{O15O11})$, $\phi_3 = \phi(\text{O15O11}[\text{Dy1}]\text{O17O9})$ and $\phi_4 = \phi(\text{O17O9}[\text{Dy1}]\text{O12O14})$, in which [Dy] represents Dy used doubly with its left two atoms and its right two atoms to form two planes, for example, $\phi(\text{O12O14}[\text{Dy1}]\text{O18O8})$ means the dihedral angle of O12O14Dy1 plane and Dy1O18O8 plane. The $d_{\text{pp}}(\text{A-B})$ means the distance between coordination A in the one plane and the other plane B. $d_{\text{pp}}^{\#}(\text{A-B})$ represented the mean value of different $d_{\text{pp}}(\text{A-B})$ values, while the d_{pp}^* value was calculated using the program Mercury by defining the centroids of the upper and lower planes and then measuring the distances of between centroids. The θ means the dihedral angle between the upper and lower planes.

Table S10. Best fitted parameters obtained for the extended Debye model with ac susceptibility data from SQUID magnetometer of compound **1** under a zero dc applied field.

$T(K)$	χ_s	χ_T	$\tau(s)$	α	Residual
1.80137	1.96219E-14	1.76809	1.44891E-5	0.25406	0.00109
2.08055	2.6894E-14	1.58717	1.48348E-5	0.24617	0.00101
2.40036	1.95686E-14	1.44668	1.41748E-5	0.26697	6.71037E-4
2.70024	1.77054E-14	1.32512	1.4305E-5	0.26643	5.19016E-4
3.00088	2.20479E-14	1.2218	1.47695E-5	0.25591	2.57314E-4
3.30059	2.6752E-14	1.13293	1.48864E-5	0.25135	1.92183E-4
3.60058	4.04169E-14	1.05583	1.51433E-5	0.2379	2.57081E-4
3.90088	4.78103E-14	0.98904	1.50835E-5	0.23287	2.65037E-4
4.20008	5.34399E-14	0.93058	1.47261E-5	0.23354	2.3244E-4

Table S11. Best fitted parameters obtained for the extended Debye model with ac susceptibility data from SQUID magnetometer of compound **1** under a 600 Oe applied field.

T	$\chi_s(\text{Total})$	χ_{T1}	$\tau_1(s)$	α_1	χ_{T2}	$\tau_2(s)$	α_2	Residual
1.8	0.12963	0.95398	3.1625E-5	1.36634E-8	0.66981	0.00131	0.21113	0.001
2.1	2.39718E-7	0.97318	2.57641E-5	2.87137E-8	0.59375	0.00111	0.19283	0.00103
2.4	2.78297E-7	0.89463	2.48247E-5	2.93387E-8	0.53735	0.00103	0.1758	0.00117
2.7	3.94359E-7	0.81769	2.40008E-5	3.23769E-8	0.50057	9.38022E-4	0.1937	9.81993E-4
3.0	4.2648E-7	0.77931	2.50445E-5	5.15524E-8	0.42442	8.6531E-4	0.14585	0.00114
3.3	5.11941E-7	0.72718	2.36267E-5	5.74981E-8	0.39289	7.67276E-4	0.14666	0.00105
3.6	6.31068E-7	0.69711	2.43439E-5	6.40084E-8	0.34268	7.16314E-4	0.10997	9.85498E-4
3.9	7.89659E-7	0.65984	2.32884E-5	9.55027E-8	0.31911	6.45443E-4	0.10987	6.23672E-4
4.2	1.20062E-6	0.62923	2.2495E-5	1.17538E-7	0.2976	5.90074E-4	0.11342	3.68535E-4
4.5	1.31251E-6	0.60265	2.22327E-5	1.37212E-7	0.27383	5.26295E-4	0.11692	2.58744E-4
4.8	1.90687E-6	0.59468	2.36595E-5	1.68623E-7	0.23273	5.0285E-4	0.0838	2.21338E-4
5.1	1.64222E-6	0.57166	2.28776E-5	1.81617E-7	0.21747	4.41716E-4	0.1076	3.08366E-4
5.4	1.30543E-6	0.569	2.38952E-5	3.0815E-7	0.17994	4.17205E-4	0.07055	1.79428E-4
5.7	1.45824E-6	0.56432	2.52692E-5	4.46865E-7	0.14876	3.96732E-4	0.06492	1.13006E-4
6.0	2.64189E-6	0.5592	2.54458E-5	4.64488E-7	0.12394	3.72945E-4	0.06424	1.18873E-4

Note: The values of α_1 were labelled with red to see easily, and the too small values obviously indicate that it is not reasonable for α_1 .

Table S12. Best fitted parameters obtained for the extended Debye model with ac susceptibility data from SQUID magnetometer of compound **1** under a 600 Oe applied field.

$T(\text{K})$	χ_s	χ_T	τ (s)	α	Residual
1.8	0.91403	1.76322	8.61574E-4	0.28455	0.00175
2.1	0.83022	1.57302	7.59847E-4	0.25302	0.00157
2.4	0.78197	1.43628	7.51273E-4	0.22455	0.00122
2.7	0.69387	1.32249	6.46576E-4	0.24727	8.26882E-4
3.0	0.65396	1.20744	5.86581E-4	0.20645	0.00105
3.3	0.6034	1.1232	5.11705E-4	0.20567	8.98117E-4
3.6	0.57722	1.0424	4.78734E-4	0.17106	9.71468E-4
3.9	0.54649	0.98111	4.33769E-4	0.16577	5.45506E-4
4.2	0.531	0.92848	4.1172E-4	0.15807	2.72521E-4
4.5	0.49949	0.87787	3.55047E-4	0.16022	1.4953E-4
4.8	0.48989	0.82856	3.33546E-4	0.12808	1.93779E-4
5.1	0.46678	0.79007	2.86498E-4	0.14397	2.42954E-4
5.4	0.45673	0.74976	2.59073E-4	0.11109	1.20725E-4
5.7	0.41957	0.71391	2.03697E-4	0.11941	6.09862E-5
6.0	0.41317	0.68379	1.82182E-4	0.11181	7.16611E-5

Table S13. Best fitted parameters obtained for the extended Debye model with ac susceptibility data from SQUID magnetometer of complex **2** in the 800 Oe applied field.

	$T(\text{K})$	χ_S	χ_T	τ (s)	α	Residual
1	1.8	1.24799E-8	2.17991	1.23352E-5	0.4413	0.00422
2	2.1	1.98958E-8	1.97918	3.76945E-6	0.53084	0.00236
3	2.4	4.79783E-8	1.75823	1.38873E-6	0.55388	0.00186
4	2.7	2.34398E-7	1.57904	4.06306E-7	0.59352	9.94526E-4
5	3.0	5.66147E-6	1.4209	1.48052E-7	0.61673	0.00105
6	3.3	1.47348E-5	1.29382	1.20124E-8	0.69373	2.99838E-4

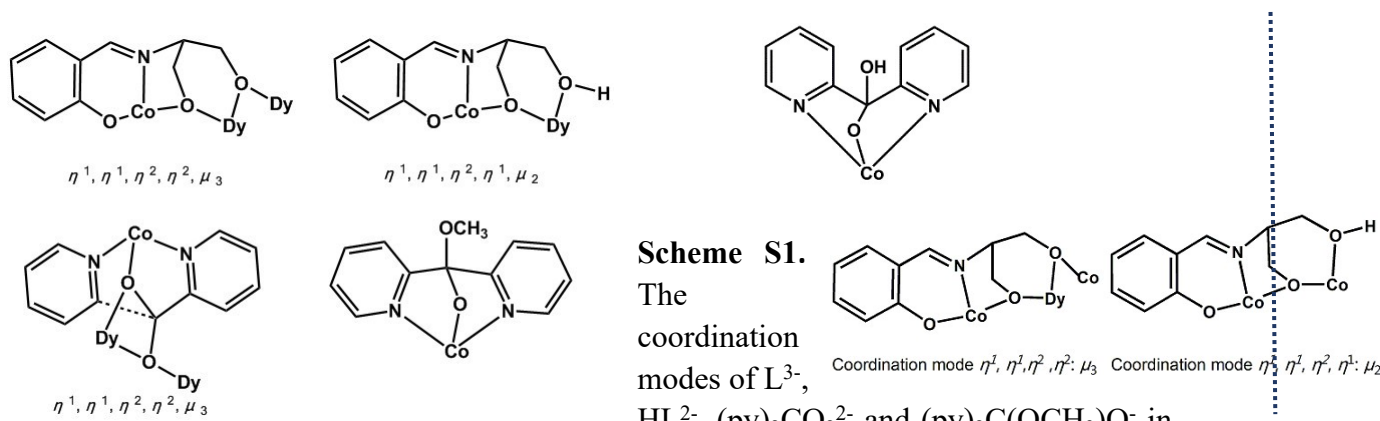
Table S14. Details of the E_a and τ_0 parameters of **2** obtained by the equation of $\ln(\chi''/\chi') = \ln(\omega\tau_0) + E_a/(k_B T)$.

Frequencies (Hz)	E_a (K)	τ_0 (s)	Frequencies (Hz)	E_a (K)	τ_0 (s)
32	5.83	4.22×10^{-6}	251	6.80	1.25×10^{-6}
45	6.22	3.24×10^{-6}	355	6.25	1.39×10^{-6}
63	6.43	2.66×10^{-6}	500	6.24	1.17×10^{-6}
89	6.72	2.03×10^{-6}	708	6.27	9.57×10^{-7}
125	6.91	1.64×10^{-6}	999	6.17	8.20×10^{-7}
177	6.93	1.39×10^{-6}	Mean values	6.43	1.89×10^{-6}

Table S15. The structural and magnetic parameters of the selected Co^{III}-Dy heterometallic complexes reported recently.

Co-Dy complex	$(U_{\text{eff}}/k_{\text{B}})/\text{K}$	Geometries	Topology	Ref.
[L ₁ Co ^{III} Br ₂ Dy ^{III} (acac) ₂]·CH ₂ Cl ₂	312.26 ⁱ	BTPR-8	Linearity	21
[L ₂ Co ^{III} Cl ₂ Dy ^{III} (acac)Cl(MeOH)]	285.04 ⁱ	BTPR-8	Linearity	21
[L ₂ Co ^{III} Cl ₂ Dy ^{III} (acac)Cl(H ₂ O)]	220.88 ⁱ	BTPR-8	Linearity	21
[Co ^{III} ₂ Dy ^{III} ₂ (OH) ₂ (bdea) ₂ (acac) ₂ (NO ₃) ₄]	169 ⁱⁱ	SAP-8	Butterfly	24
[Co ^{III} ₂ Dy ^{III} ₂ (OMe) ₂ (teaH) ₂ (piv) ₆]	127 ⁱ	SAP-8	Butterfly	25
[Co ^{III} ₂ Dy ^{III} ₂ (μ ₃ -OH) ₂ (o-tol) ₄ (mdea) ₂ (NO ₃) ₂]	116.9 ⁱ	SAP-8	Butterfly	27
[Co ^{III} ₄ Dy ^{III} ₂ (OH) ₂ (teaH) ₂ (tea) ₂ (piv) ₆]	78 ⁱ	SAP-8	Not reported	32
[Co ^{III} ₂ Dy ^{III} ₂ (L ₃) ₂ (pdm) ₂ (CH ₃ COO) ₂ (CH ₃ OH) ₂](NO ₃) ₂	64.0(9) ^{a,i}	MFF-9	Linearity	29
[Co ^{III} ₂ Dy ^{III} ₂ (HL)L{(py) ₂ CO ₂ }{(py) ₂ C(OCH ₃)O}(NO ₃) ₄ CH ₃ OH]·solv	59.4 ^{b,i} (U ₁)	TDD-8, MFF-9	Star	*
.				
[Co ^{III} Dy ^{III} ₃ (HBpz ₃) ₆ (dto) ₃]·4CH ₃ CN·2CH ₂ Cl ₂	52 ^{c,ii}	SAP-8	Propeller	22
[Co ^{III} ₄ Dy ^{III} ₃ L ₄ (μ ₄ -O) ₂ (μ-OMe) ₂ (μ _{1,3} -OAc) ₄ (H ₂ O) ₂ (NO ₃) ₂]·NO ₃ ·sol.	51.4 ⁱⁱⁱ	JTCTPR-9	Sand clock	33
[Dy ^{III} ₂ Co ^{III} ₂ (OH) ₂ (teaH) ₂ (acac) ₆]·MeCN	45 ⁱⁱ (U ₁)	SAP-8	Butterfly	26
[Co ^{III} ₄ Dy ^{III} ₄ (μ-F) ₄ (μ ₃ -OH) ₄ (o-tol) ₈ (mdea) ₄]	39 ⁱⁱ	BTP-8	Square	34
[Dy ^{III} ₂ Co ^{III} ₂ (OH) ₂ (bdea) ₂ (acac) ₆]·2H ₂ O	38 ⁱⁱ	SAP-8	Butterfly	26
[Co ^{III} ₂ Dy ^{III} ₂ (L ₃) ₂ (CH ₃ COO) ₄ (OH) ₂ (H ₂ O) ₂](ClO ₄) ₂	33.8 ⁱⁱ	TCTPR-9	Linearity	30
[Co ^{III} ₂ Dy ^{III} ₄ (μ ₃ -OH) ₂ (NO ₃) ₄ (OAc) ₄ L ₄ (DMF) ₂]	31.6 ⁱⁱ	SAP-8	Chair-like	31
[Dy ^{III} ₂ Co ^{III} ₂ (OH) ₂ (edea) ₂ (acac) ₆]·2H ₂ O·4MeCN	16 ⁱⁱ	SAP-8	Butterfly	26
[Co ^{III} ₂ Dy ^{III} ₂ (OCH ₃) ₂ (teaH) ₂ (piv) ₆]	none	SAP-8	Butterfly	28

The parameters of the complex reported in this work was labeled by red. ⁱ U_{eff} obtained by the equation of $\tau^{-1} = CT^n + \tau_0^{-1}\exp(-U_{\text{eff}}/k_{\text{B}}T) + \tau_{\text{QTM}}^{-1}$; ⁱⁱ U_{eff} obtained by the equation of $\tau = \tau_0\exp(U_{\text{eff}}/k_{\text{B}}T)$; ⁱⁱⁱenergy barrier (E_a) obtained employing the equation $\ln(\chi''/\chi') = \ln(\omega\tau_0) + E_a/(k_{\text{B}}T)$. ^{a, b, c}show the ac susceptibility data measured under 2000, 600 and 800 Oe dc fields, respectively. BTPR-8 = biaugmented trigonal prism; SAP-8 = square antiprism; JTCTPR-9 = Tricapped trigonal prism (J51); TCTPR-9 = Tricapped trigonal prism; TDD-8 = triangular dodecahedron; MFF-9 = muffin. H₂L₁ = N,N'-bis(2-oxy-3-methoxybenzylidene)-1,2-phenyl-enediamine; H₂L₂ = N,N'-bis(2-oxy-3-methoxybenzylidene)-1,2-diaminocyclohexane; H₂L₃ = N1,N3-bis(3-methoxysalicylidene)diethylenetriamine; H₂L₄ = 3-methoxysalicylaldehyde and 2-amino-2-methyl-1-propanol; acac = acetylacetonate; bdeaH₂ = *n*-butyldiethanolamine; teaH₃ = triethanolamine; Hpiv = pivalic acid; o-tol = o-toluate; mdeaH₂ = N-methyldiethanolamine; pdmH₂ = 2,6-pyridinedimethanol; HBpz₃⁻ = hydrotris(pyrazolyl)borate; dto²⁻ = dithiooxalato dianion; edeaH₂ = N-ethyl-diethanolamine.



1 (left) and **L**³⁻, **HL**²⁻ as well as **(py)**₂**C(OH)O**⁻ in **2** (right).

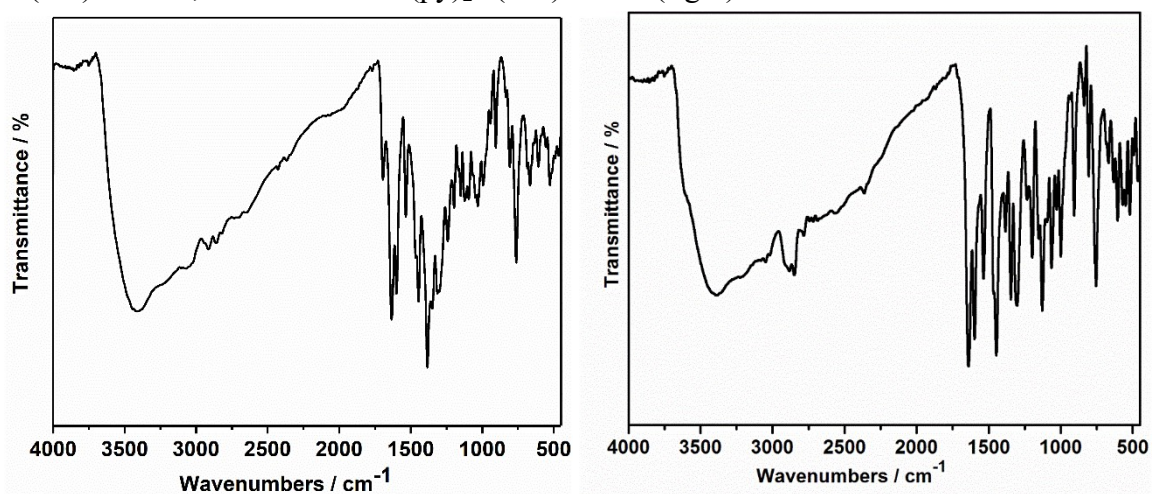


Figure S1. IR spectra of **1** (left) and **2** (right).

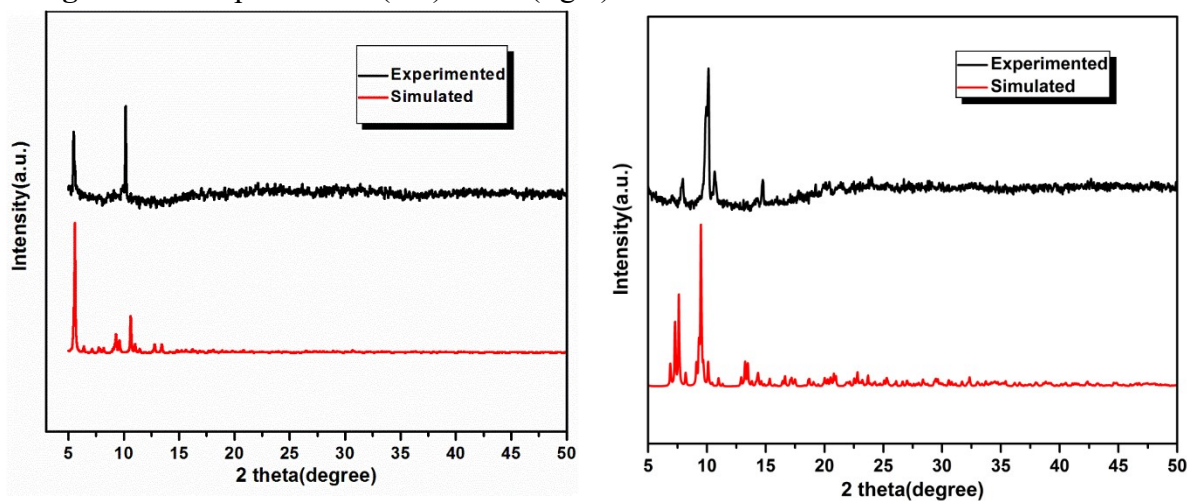


Figure S2. Experimental and simulated Powder X-ray diffraction (PXRD) of **1** (left) and **2** (right). Some peaks. Some minor peaks were lost, which could be due to the loss of some solvent molecules in the crystal lattice.

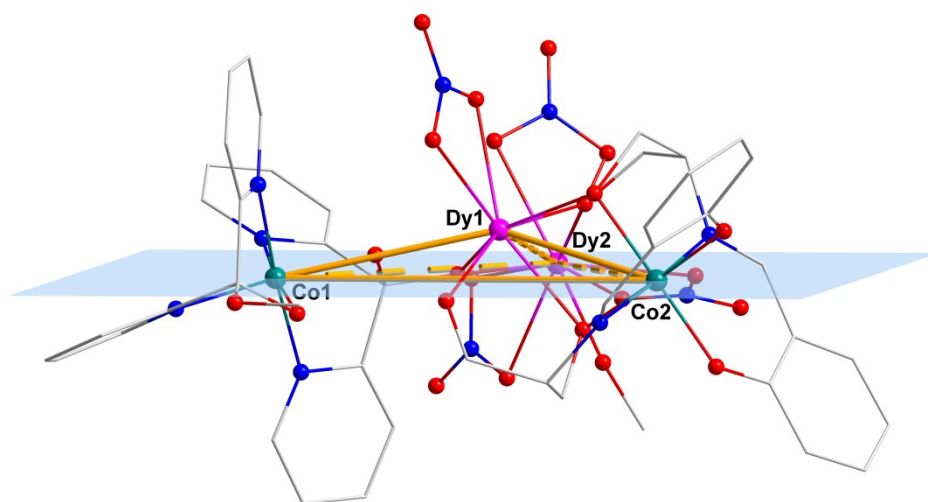


Figure S3. Plot shown two Co^{III} and two Dy^{III} of **1** in a shrinking trigonal pyramid.

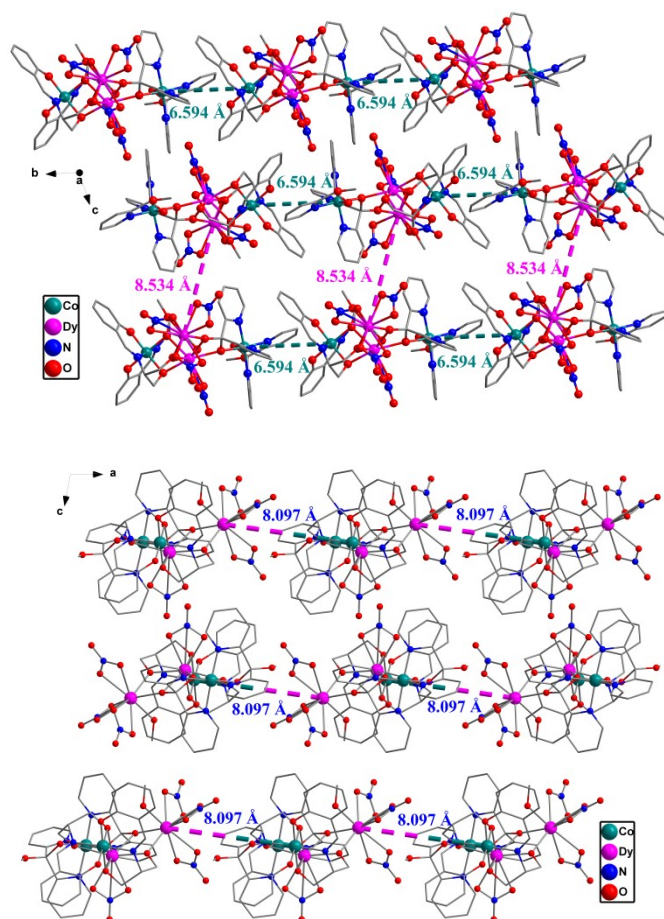


Figure S4. The plots shown the distances of the Co^{III}...Co^{III} (teal, top), Dy^{III}...Dy^{III} (pink, top) and Dy^{III}...Co^{III} (blue, bottom) between molecules of **1** in the crystal lattice.

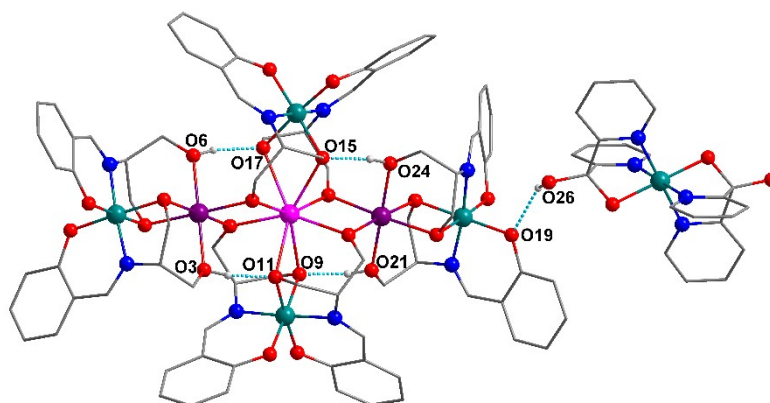


Figure S5. The intramolecular H bonds between the nondeprotonated hydroxyl groups and the neighboring O atoms in **2**.

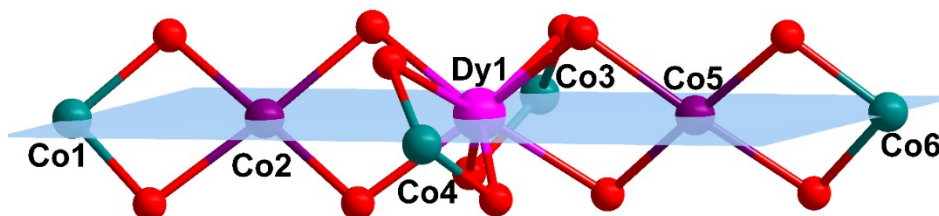


Figure S6. The plot shown the all metal ions in the $[\text{Co}^{\text{II}}_2\text{Co}^{\text{III}}_4\text{Dy}^{\text{III}}(\text{HL})_4(\text{L})_4]^-$ anion of **1**.

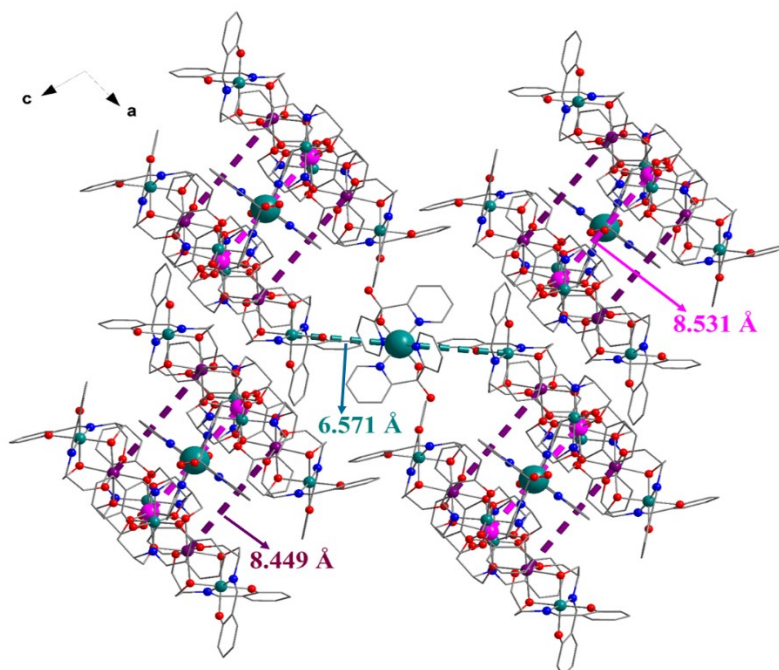


Figure S7. The plot shown the distances of the $\text{Co}^{\text{III}}\cdots\text{Co}^{\text{III}}$ (teal), $\text{Co}^{\text{II}}\cdots\text{Co}^{\text{II}}$ (violet) and $\text{Dy}^{\text{III}}\cdots\text{Dy}^{\text{III}}$ (pink) between molecules of **1**.

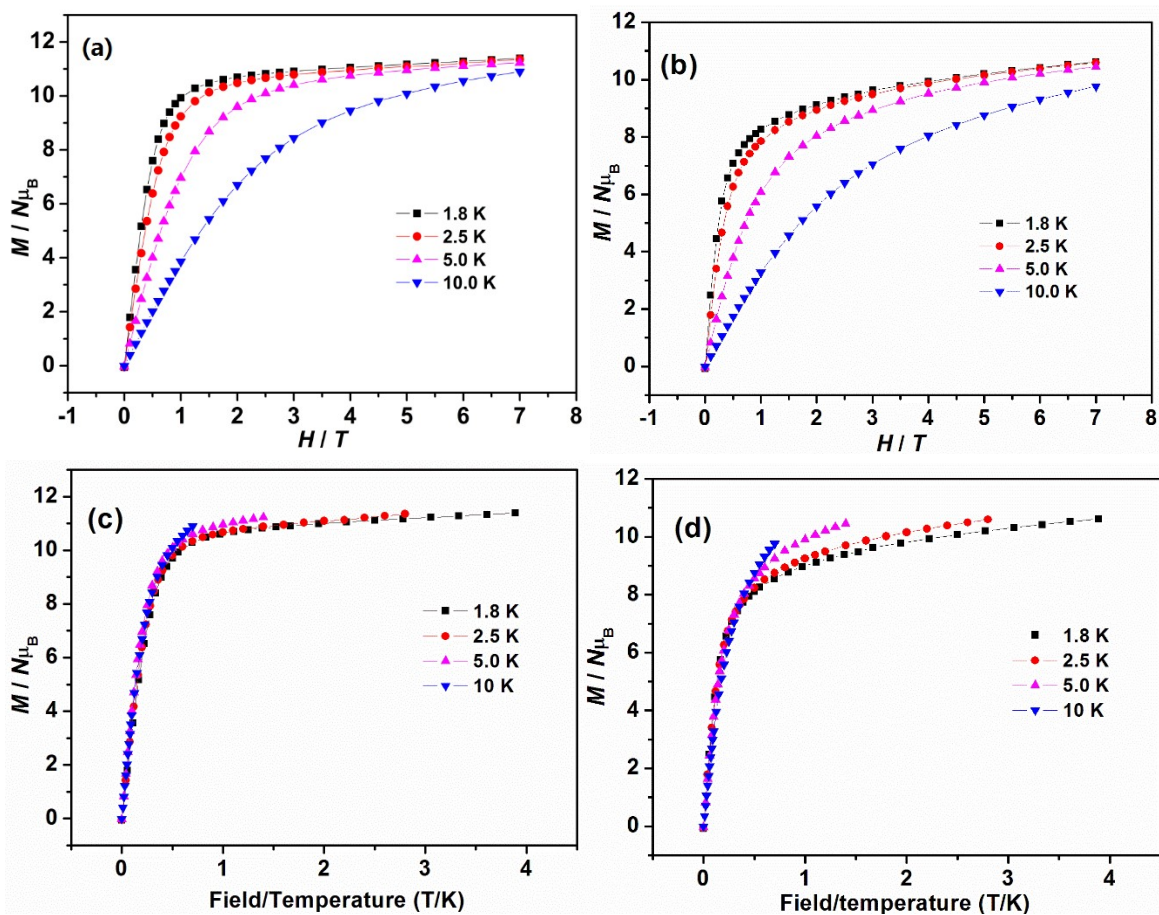


Figure S8. The plots of M vs. H for **1** (a) and **2** (b) and the plots of M vs. H/T for **1** (c) and **2**(d).

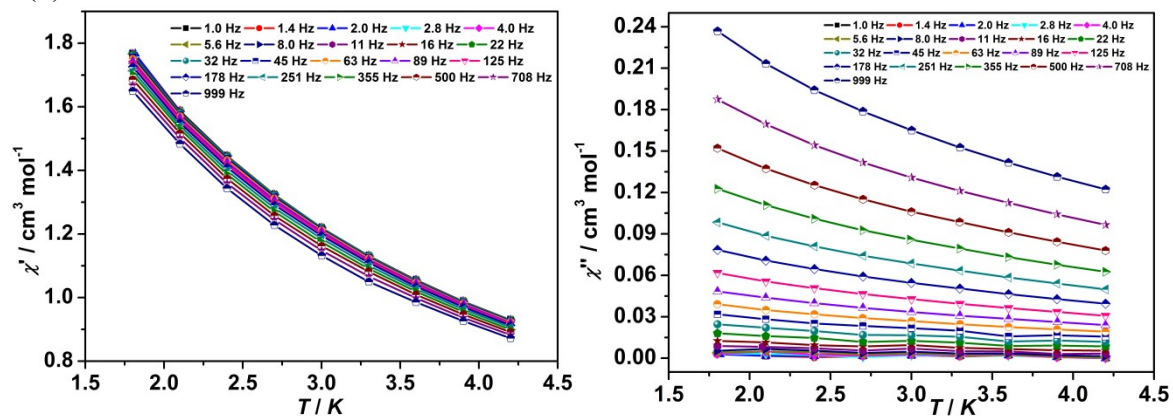


Figure S9. The temperature dependence of the in-phase (χ' , left) and out-of-phase (χ'' , right) ac susceptibilities of **1** measured under a zero dc field.

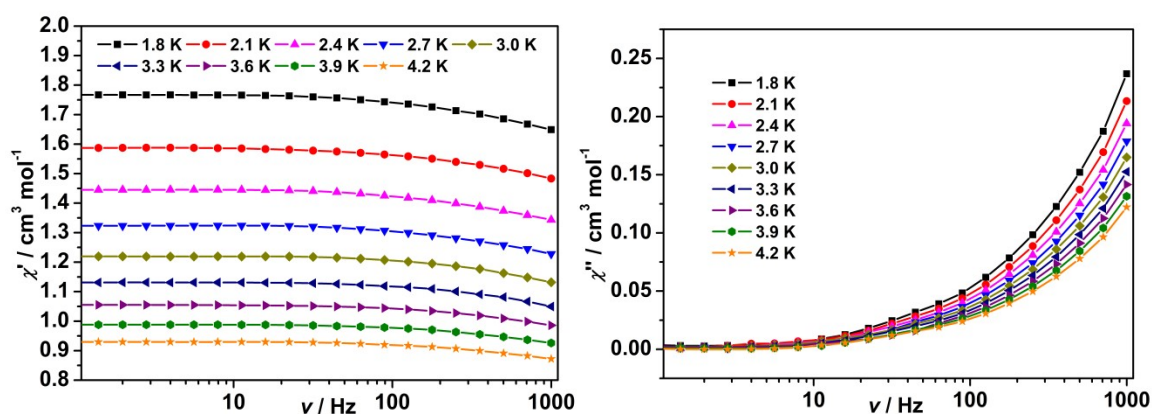


Figure S10. The frequency dependence of the in-phase (χ' , left) and out-of-phase (χ'' , right) ac susceptibilities of **1** measured under a zero dc field.

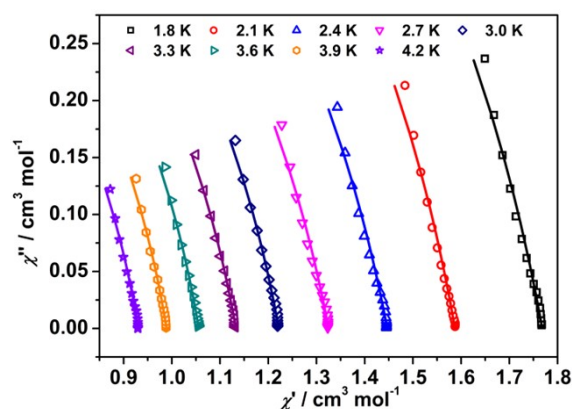


Figure S11. Cole-Cole plots of **1** measured under a zero dc field, in which solid lines represent the fitted results by the single relaxation Debye model.

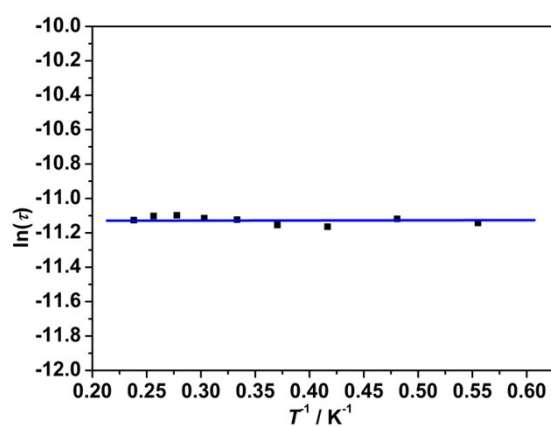


Figure S12. Plots of $\ln(\tau)$ vs. T^{-1} for **1** measured under a zero dc field, in which the blue line to see easily and it is almost parallel T^{-1} axis, indicating that the slow magnetic relaxation behavior under a zero dc field was almost governed by pure quantum tunnelling of magnetization (QTM) process.

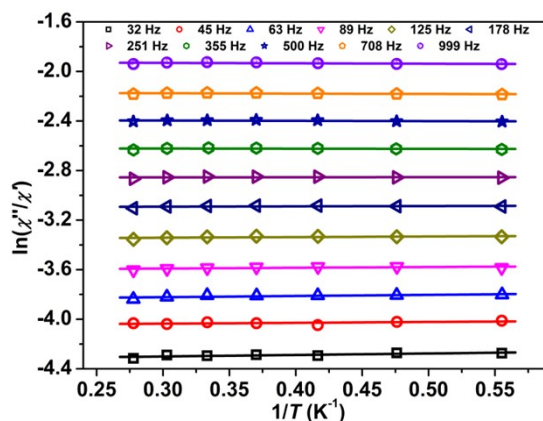


Figure S13. Linear approximation plots of (χ''/χ') vs T^{-1} at different frequencies for **1** measured under a zero dc field, the solid lines represent the fitted results by Bartolomé equation $\ln(\chi''/\chi') = \ln(\omega\tau_0) + E_a/(k_B T)$.

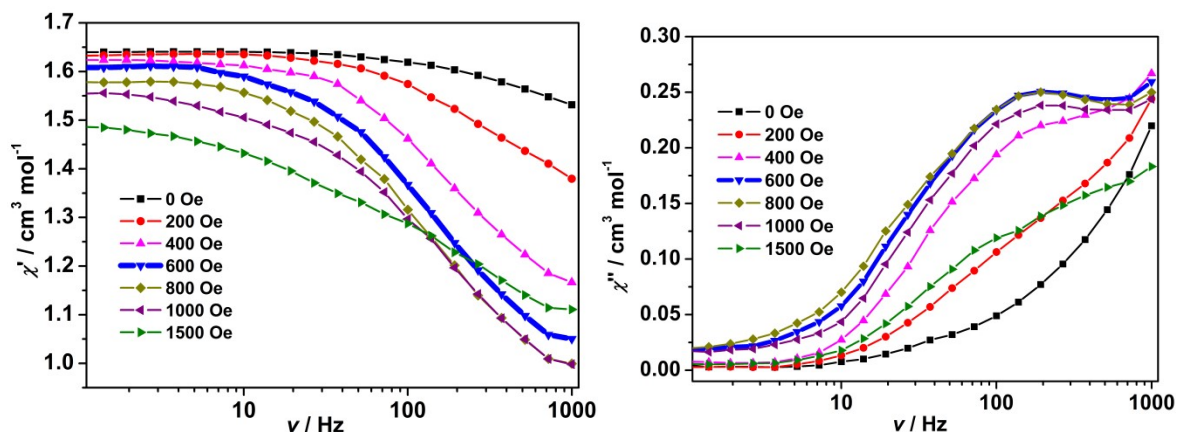


Figure S14. Frequency dependence of in-phase (χ' , a) and out-of-phase (χ'' , b) ac signals for **1** under different dc fields at 1.8 K.

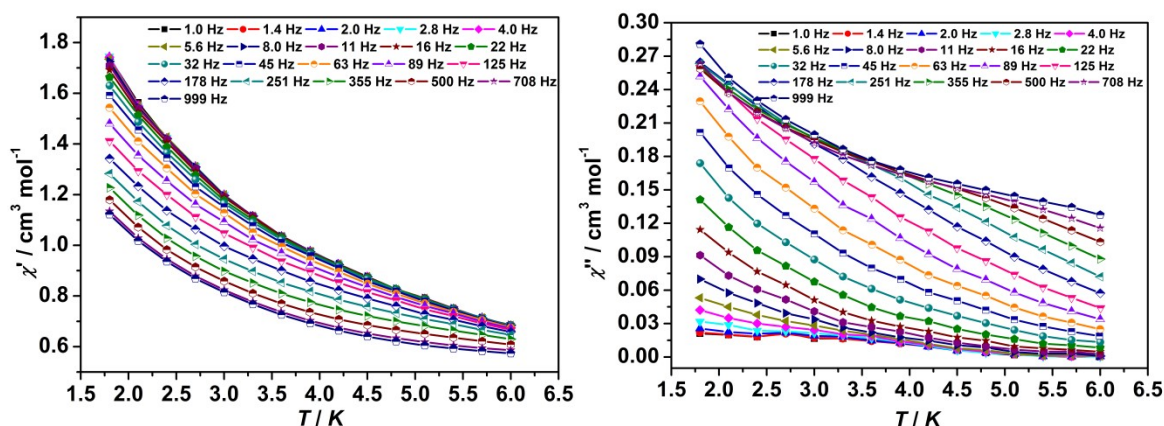


Figure S15. The temperature dependence of the in-phase (χ' , left) and out-of-phase (χ'' , right) ac susceptibilities of **1** measured under a 600 Oe dc field.

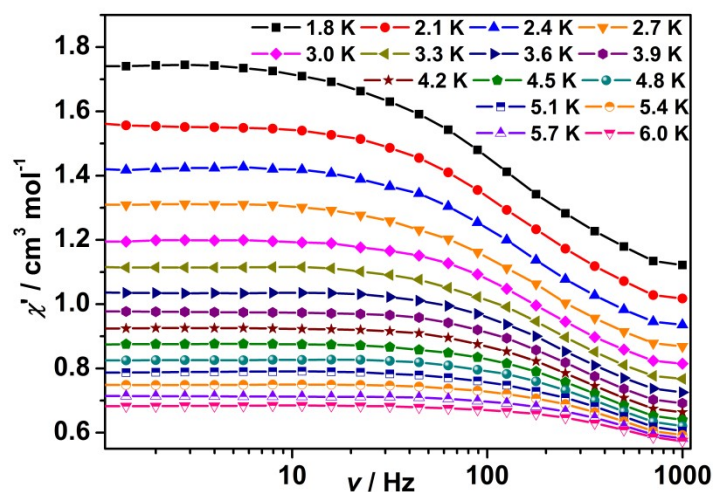


Figure S16. The frequency dependence of the in-phase (χ') ac susceptibilities of **1** measured under a 600 Oe dc field.

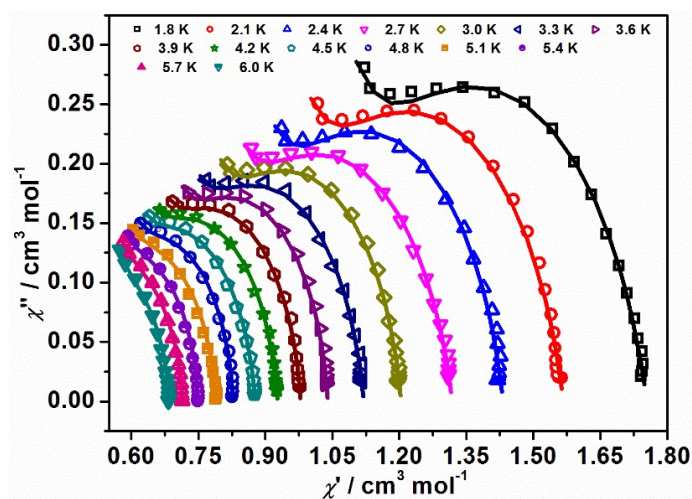


Figure S17. Cole-Cole plots of **1** measured under a 600 Oe dc field, in which solid lines represent the fitted results by the double relaxation Debye model.

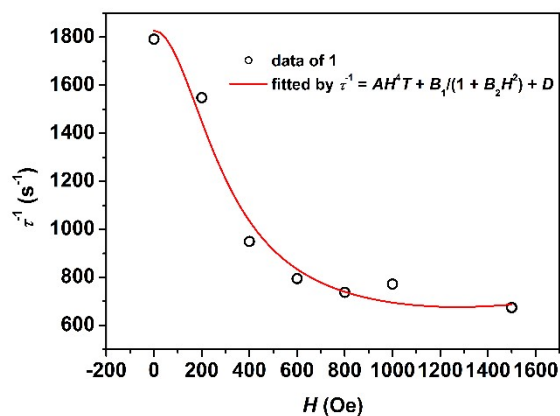


Figure S18. The plots of τ^{-1} vs. H for **1**, in which the red solid line represents the fitted results by $\tau^{-1} = AH^4T + B_1/(1 + B_2H^2) + D$.

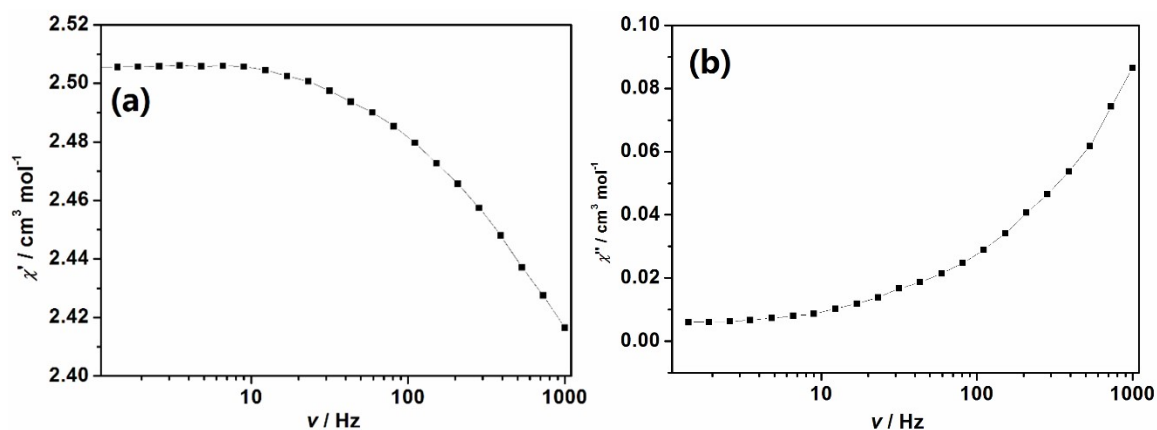


Figure S19. Plots of in-phase (χ' , a) and out-of-phase (χ'' , b) versus ν (ν represents frequencies) for **2** under zero dc field at 1.8 K.

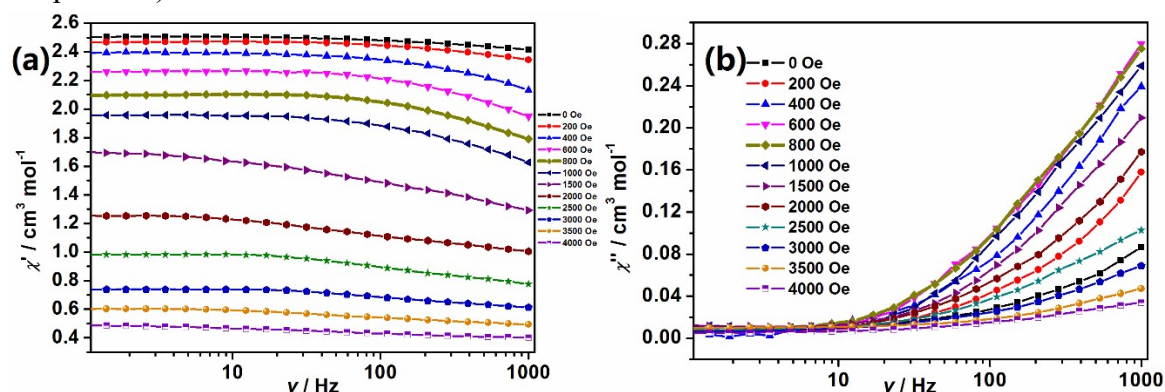


Figure S20. Frequency dependence of in-phase (χ' , a) and out-of-phase (χ'' , b) ac signals for **2** under different dc fields at 1.8 K.

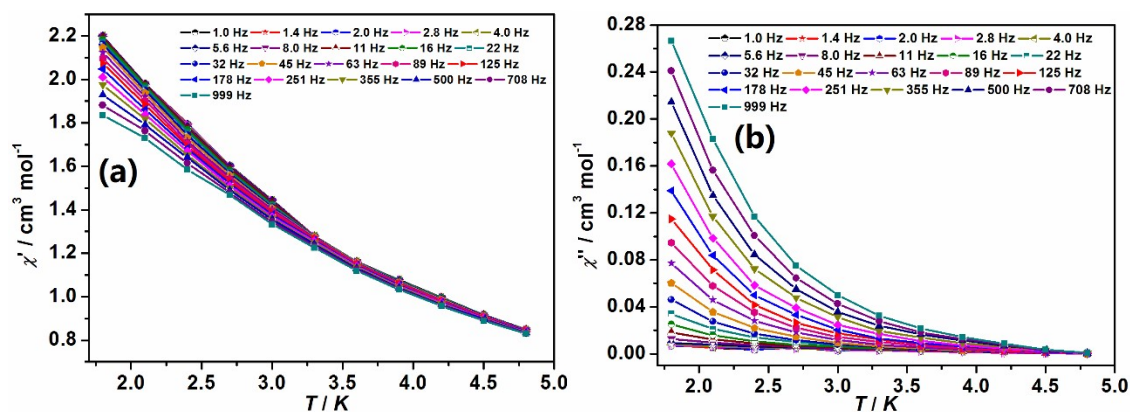


Figure S21. Temperature-dependence of in-phase (χ' , a) and out-of-phase (χ'' , b) ac signals for **2** under an 800 Oe dc field with the temperatures in the range of 1.8-4.8 K.

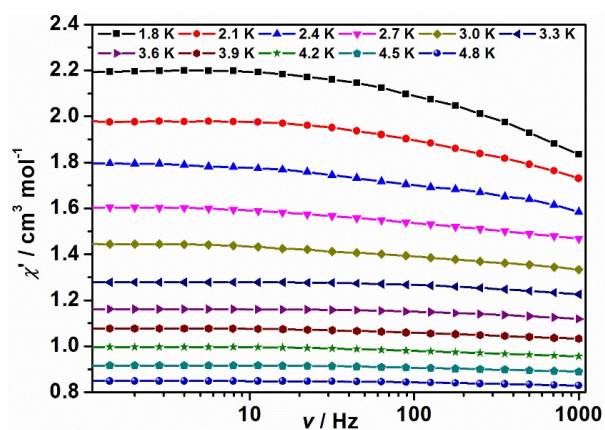


Figure S22. Plots of in-phase (χ') versus ν (ν represents frequencies) for **2** under an 800 Oe dc field with the temperatures in the range of 1.8-4.8 K.

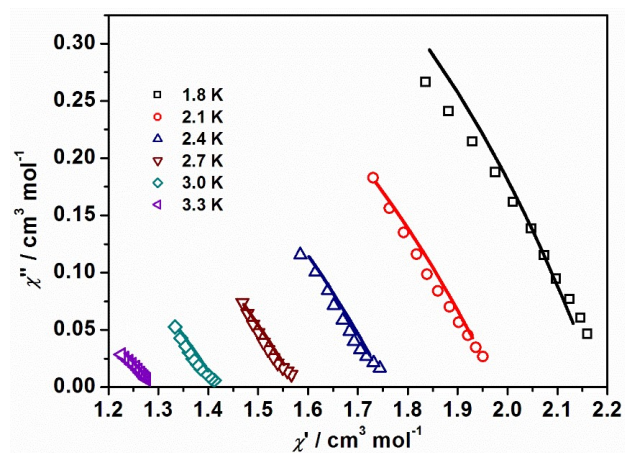


Figure S23. Cole-Cole plots for **2** measured under an 800 Oe dc field, the solid lines represent the fitted results by the single relaxation Debye model.

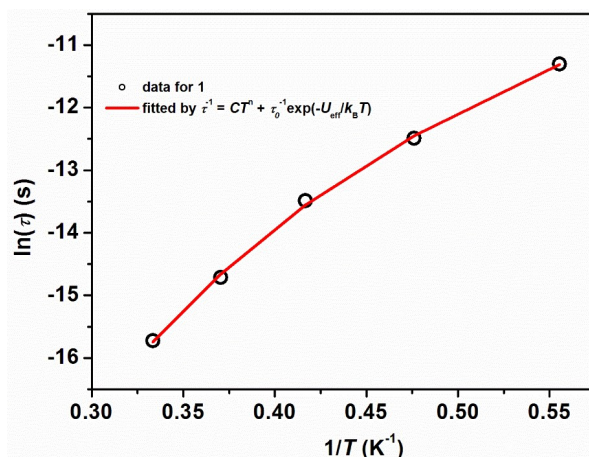


Figure S24. $\ln(\tau)$ versus T^{-1} for **2** measured under an 800 Oe dc field, the solid lines represent the fitted results by the equation of $\tau^{-1} = CT^n + \tau_0^{-1}\exp(-U_{\text{eff}}/k_B T)$.

Computational details

Complex **1** has two individual Dy^{III} ions, which were indicated as **1_Dy1** and **1_Dy2**, respectively (Figure. S24). However, complex **2** contains one Dy^{III} and two Co^{II}, so their fragments were labeled as **2_Dy**, **2_Co1** and **2_Co2**, respectively (Figure S25). Complete-active-space self-consistent field (CASSCF) calculations on **1_Dy1** and **1_Dy2** for **1** and **2_Dy**, **2_Co1** and **2_Co2** for **2** on the basis of single-crystal X-ray determined geometries have been carried out with MOLCAS 8.4^{S1} program package. All Co^{III} ions are replaced with Sc^{III} during the calculation processes. **1_Dy1**, **1_Dy2** and **2_Dy** were calculated respectively keeping the experimentally determined structures of the corresponding compound while replacing the other Dy^{III} ion with diamagnetic Lu^{III}. **2_Co1** and **2_Co2** were calculated keeping the experimentally determined structures of the corresponding compounds while replacing the other Co^{II} ion with diamagnetic Zn^{II} and Dy^{III} ion with diamagnetic Lu^{III}.

For the first CASSCF calculation, the basis sets for all atoms are atomic natural orbitals from the MOLCAS ANO-RCC library: ANO-RCC-VTZP for Dy^{III} and Co^{II}; VTZ for close O atoms; VDZ for distant atoms. The calculations employed the second order Douglas-Kroll-Hess Hamiltonian, where scalar relativistic contractions were taken into account in the basis set. And then, the spin-orbit couplings were handled separately in the restricted active space state interaction (RASSI-SO) procedure. For the individual Dy^{III} fragment, active electrons in 7 active orbitals include all *f* electrons (CAS (9 in 7)) in the CASSCF calculation. To exclude all the doubts, we calculated all the roots in the active space. We have mixed the maximum number of spin-free state which was possible with our hardware (all from 21 sextets, 128 from 224 quadruplets, 130 from 490 doublets). For the individual Co^{II} fragment, active electrons in 5+5' active orbitals include all *d* electrons (CAS (7 in 5+5')) in the CASSCF calculations. We have mixed the maximum number of spin-free states (all from 10

quadruplets and all from 40 doublets for Co^{II}). SINGLE_ANISO^[S2-S4] program was used to obtain the energy levels, **g** tensors, m_J values, spin-free energies, spin-orbit energies, magnetic axes, *et al.* based on the above CASSCF/RASSI-SO calculations.

To fit the exchange interactions between the magnetic centers in complexes **1** and **2**, we took two steps to obtain them. Firstly, we calculated individual Dy^{III} and Co^{II} fragments using CASSCF/RASSI-SO to obtain the corresponding magnetic properties. Then, the exchange interactions between the magnetic centers were considered within the Lines model,^{S5} while the account of the dipole-dipole magnetic coupling was treated exactly. The Lines model is effective and has been successfully used widely in the research field of *d* and *f*-elements single-molecule magnets.^{S6,S7}

For complex **1**, there is only one type of \mathcal{J}° (Figure S26), so the Ising exchange Hamiltonians for **1** is:

$$H_{exch} = -\tilde{J} \hat{S}_{Dy1} \hat{S}_{Dy2}$$

However, for **2**, two types of \mathcal{J}° were fitted due to asymmetry (Figure S27), and the Ising exchange Hamiltonian is:

$$H_{exch} = -\tilde{J}_1 \hat{S}_{Dy} \hat{S}_{Co1} - \tilde{J}_2 \hat{S}_{Dy} \hat{S}_{Co2}$$

In complexes **1** and **2**, $\mathcal{J}^{\circ} = 25 \cos \varphi J$ and $\tilde{J} = 15 \cos \varphi J$, respectively, where φ is the angles between the anisotropy axes on two Dy^{III} sites or between the anisotropy axes on Dy^{III} and Co^{II} sites, and J is the Lines exchange coupling parameter. $\mathcal{J}_{total}^{\circ}$ is the parameter of the total magnetic interaction ($\mathcal{J}_{total}^{\circ} = \mathcal{J}_{dip}^{\circ} + \mathcal{J}_{exch}^{\circ}$) between magnetic center ions. $\tilde{S}_{Dy} = \tilde{S}_{Co} = 1/2$ shows the ground pseudospin values of the Dy^{III} and Co^{II} sites. The dipolar magnetic coupling can be calculated exactly, while the exchange coupling constant was fitted through comparison of the computed and measured magnetic susceptibilities using POLY_ANISO program.^{S2-S4}

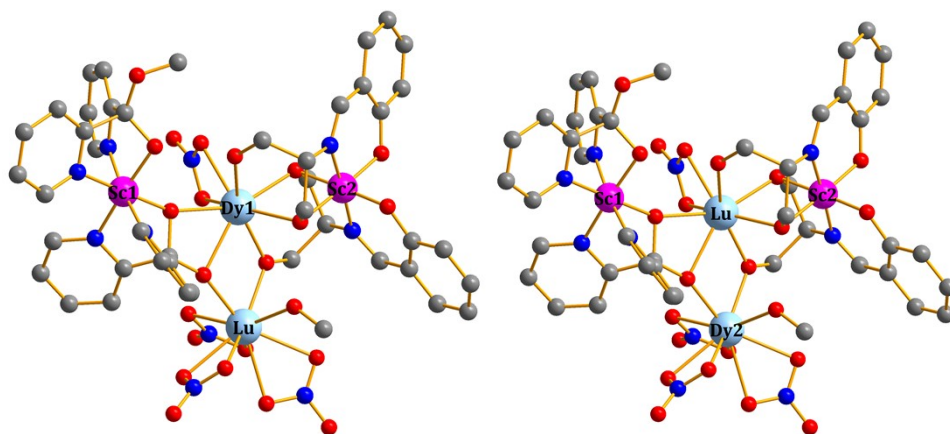


Figure S25. Calculated complete structures of **1_Dy1** (left) and **1_Dy2** (right); H atoms are omitted for clarify.

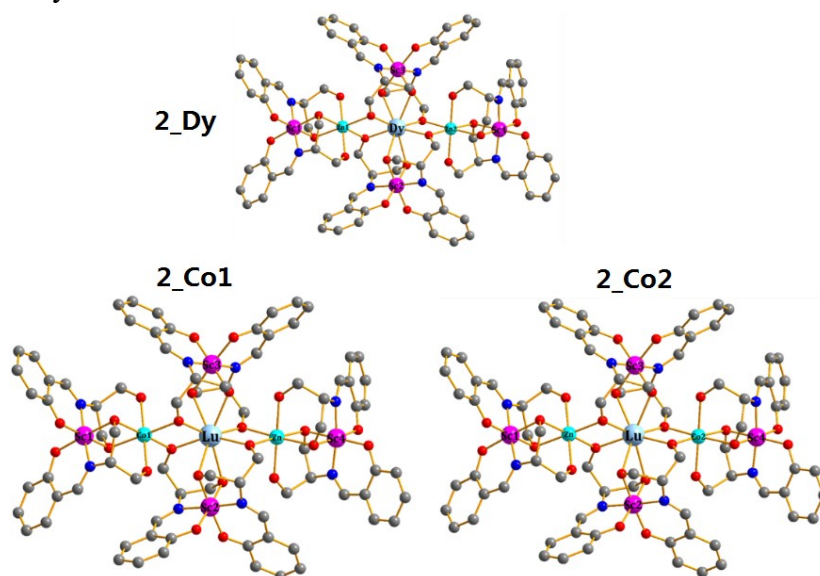


Figure S26. Calculated models of **2_Dy**, **2_Co1** and **2_Co2** for **2**. H atoms are omitted for clarify.

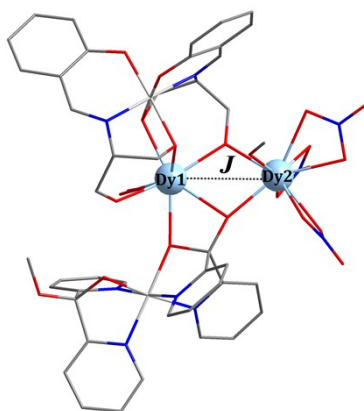


Figure S27. Scheme of the Dy^{III}...Dy^{III} anisotropic interaction in **1**.

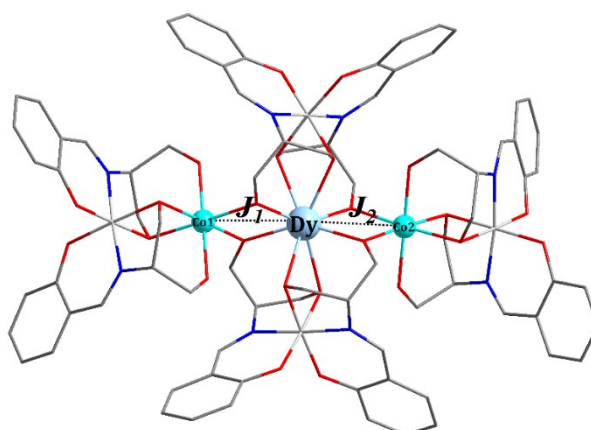


Figure S28. Scheme of the Dy^{III}...Co^{II} anisotropic interactions in **2**.

Table S16. Wave functions with definite projection of the total moment $|m_J\rangle$ for the lowest eight KDs of **1_Dy1**, **1_Dy2** and **2_Dy** using CASSCF/RASSI-SO with MOLCAS 8.4.

	E/cm^{-1}	wave functions
1_Dy1	0.0	98.4% $ \pm 15/2\rangle$
	97.9	23.8% $ \pm 13/2\rangle$ +22.5% $ \pm 11/2\rangle$ +22.1% $ \pm 9/2\rangle$ +13.8% $ \pm 7/2\rangle$ +7.8% $ \pm 5/2\rangle$
	165.2	34.3% $ \pm 13/2\rangle$ +19.5% $ \pm 3/2\rangle$ +14.4% $ \pm 7/2\rangle$ +13.6% $ \pm 5/2\rangle$ +10.1% $ \pm 1/2\rangle$
	224.3	28.3% $ \pm 1/2\rangle$ +19.9% $ \pm 5/2\rangle$ +15.3% $ \pm 13/2\rangle$ +11.5% $ \pm 7/2\rangle$ +8.8% $ \pm 9/2\rangle$ +8.1% $ \pm 11/2\rangle$
	264.9	35.9% $ \pm 3/2\rangle$ +28.8% $ \pm 1/2\rangle$ +12.0% $ \pm 13/2\rangle$ +11.9% $ \pm 5/2\rangle$ +7.9% $ \pm 11/2\rangle$
	351.8	26.8% $ \pm 5/2\rangle$ +18.7% $ \pm 1/2\rangle$ +17.2% $ \pm 3/2\rangle$ +14.4% $ \pm 7/2\rangle$ +9.5% $ \pm 11/2\rangle$ +8.6% $ \pm 13/2\rangle$
	405.2	33.5% $ \pm 11/2\rangle$ +32.2% $ \pm 9/2\rangle$ +15.9% $ \pm 7/2\rangle$ +7.7% $ \pm 3/2\rangle$ +6.8% $ \pm 1/2\rangle$
	570.2	27.9% $ \pm 7/2\rangle$ +27.2% $ \pm 9/2\rangle$ +19.3% $ \pm 5/2\rangle$ +13.1% $ \pm 11/2\rangle$ +7.5% $ \pm 3/2\rangle$
1_Dy2	0.0	99.3% $ \pm 15/2\rangle$
	214.4	84.0% $ \pm 13/2\rangle$ +5.9% $ \pm 5/2\rangle$ +4.5% $ \pm 1/2\rangle$
	263.0	26.9% $ \pm 3/2\rangle$ +20.0% $ \pm 11/2\rangle$ +18.6% $ \pm 1/2\rangle$ +16.7% $ \pm 9/2\rangle$ +6.7% $ \pm 5/2\rangle$ +5.7% $ \pm 13/2\rangle$
	291.9	23.5% $ \pm 7/2\rangle$ +19.5% $ \pm 1/2\rangle$ +18.4% $ \pm 5/2\rangle$ +18.0% $ \pm 11/2\rangle$ +7.5% $ \pm 9/2\rangle$ +6.7% $ \pm 13/2\rangle$
	340.2	32.8% $ \pm 11/2\rangle$ +27.1% $ \pm 9/2\rangle$ +13.4% $ \pm 5/2\rangle$ +9.9% $ \pm 3/2\rangle$ +9.3% $ \pm 7/2\rangle$
	392.9	24.3% $ \pm 7/2\rangle$ +24.3% $ \pm 3/2\rangle$ +16.2% $ \pm 11/2\rangle$ +14.5% $ \pm 5/2\rangle$ +12.0% $ \pm 9/2\rangle$
	424.9	29.0% $ \pm 1/2\rangle$ +21.3% $ \pm 5/2\rangle$ +18.8% $ \pm 9/2\rangle$ +12.3% $ \pm 7/2\rangle$ +9.1% $ \pm 11/2\rangle$
	473.7	23.0% $ \pm 7/2\rangle$ +21.8% $ \pm 3/2\rangle$ +19.8% $ \pm 5/2\rangle$ +17.5% $ \pm 9/2\rangle$ +15.0% $ \pm 1/2\rangle$
2_Dy	0.0	62.8% $ \pm 15/2\rangle$ +11.0% $ \pm 13/2\rangle$ +8.1% $ \pm 9/2\rangle$ +6.9% $ \pm 11/2\rangle$ +4.7% $ \pm 5/2\rangle$
	13.7	23.7% $ \pm 7/2\rangle$ +17.4% $ \pm 13/2\rangle$ +17.1% $ \pm 5/2\rangle$ +12.5% $ \pm 9/2\rangle$ +11.3% $ \pm 15/2\rangle$ +9.9% $ \pm 3/2\rangle$
	132.1	62.1% $ \pm 13/2\rangle$ +20.4% $ \pm 15/2\rangle$ +5.6% $ \pm 5/2\rangle$ +4.8% $ \pm 1/2\rangle$
	160.2	53.3% $ \pm 11/2\rangle$ +14.4% $ \pm 3/2\rangle$ +10.2% $ \pm 9/2\rangle$ +7.4% $ \pm 5/2\rangle$ +6.3% $ \pm 1/2\rangle$
	213.7	23.2% $ \pm 9/2\rangle$ +23.1% $ \pm 11/2\rangle$ +14.4% $ \pm 7/2\rangle$ +12.9% $ \pm 3/2\rangle$ +11.1% $ \pm 1/2\rangle$ +6.9% $ \pm 5/2\rangle$
	270.0	38.9% $ \pm 1/2\rangle$ +23.1% $ \pm 5/2\rangle$ +20.3% $ \pm 19/2\rangle$ +5.7% $ \pm 7/2\rangle$ +5.6% $ \pm 11/2\rangle$
	312.9	34.9% $ \pm 3/2\rangle$ +30.1% $ \pm 1/2\rangle$ +19.1% $ \pm 7/2\rangle$ +12.4% $ \pm 9/2\rangle$
	518.8	33.0% $ \pm 5/2\rangle$ +28.2% $ \pm 7/2\rangle$ +18.0% $ \pm 3/2\rangle$ +12.3% $ \pm 9/2\rangle$

Table S17. Calculated energy levels (cm^{-1}), \mathbf{g} (g_x, g_y, g_z) tensors and predominant m_J values of the lowest eight Kramers doublets (KDs) of **1_Dy1**, **1_Dy2** and **2_Dy** using CASSCF/RASSI-SO with MOLCAS 8.4.

KDs	1_Dy1			1_Dy2			2_Dy		
	E/cm^{-1}	\mathbf{g}	m_J	E/cm^{-1}	\mathbf{g}	m_J	E/cm^{-1}	\mathbf{g}	m_J
1	0.0	0.001	$\pm 15/2$	0.0	0.004	$\pm 15/2$	0.0	0.076	$\pm 15/2$
		0.062			0.009			1.575	
		19.720			19.811			16.908	
2	97.9	0.612	$\pm 13/2$	214.4	0.908	$\pm 13/2$	13.7	0.059	$\pm 7/2$
		0.819			1.831			1.591	
		16.670			15.263			16.192	
3	165.2	2.726	$\pm 13/2$	263.0	2.383	$\pm 3/2$	132.1	1.183	$\pm 13/2$
		3.555			6.136			1.301	
		13.071			11.439			16.449	
4	224.3	0.547	$\pm 1/2$	291.9	2.059	$\pm 7/2$	160.2	1.771	$\pm 11/2$
		5.250			5.740			3.547	
		10.637			9.696			13.199	
5	264.9	3.527	$\pm 3/2$	340.2	8.963	$\pm 11/2$	213.7	1.903	$\pm 9/2$
		5.049			7.218			6.308	
		12.739			3.608			11.125	
6	351.8	0.254	$\pm 5/2$	392.9	0.759	$\pm 7/2$	270.0	0.971	$\pm 1/2$
		2.128			2.505			3.724	
		13.070			13.184			9.574	
7	405.2	0.335	$\pm 11/2$	424.9	1.061	$\pm 1/2$	312.9	0.657	$\pm 3/2$
		1.363			2.209			1.668	
		16.460			15.221			12.722	
8	570.2	0.053	$\pm 7/2$	473.7	0.421	$\pm 7/2$	518.8	0.017	$\pm 5/2$
		0.105			0.634			0.039	
		19.468			18.668			19.333	

Table S18. Calculated spin-free energies (cm^{-1}) of the lowest ten terms ($S = 3/2$) of **2_Co1** and **2_Co2** using CASSCF/RASSI-SO with MOLCAS 8.4.

KDs	2_Co1 (E/cm^{-1})	2_Co2 (E/cm^{-1})
1	0.0	0.0
2	373.6	402.5
3	1112.4	1115.6
4	6355.8	6276.4
5	6994.9	7002.3
6	7696.3	7667.8
7	14679.5	14600.2
8	22779.6	22753.7
9	24133.7	24064.6
10	25464.5	25491.8

Table S19. Calculated weights of the five most important spin-free states for the lowest two spin-orbit states of **2_Co1** and **2_Co2** using CASSCF/RASSI-SO with MOLCAS 8.4.

	Spin-orbit states	Energy (cm^{-1})	Spin-free states, Spin, Weights				
2_Co1	1	0.0	1,1.5,0.6487	2,1.5,0.2941	3,1.5,0.0538	4,1.5,0.0011	5,1.5,0.0006
	2	210.1	1,1.5,0.8574	2,1.5,0.0988	3,1.5,0.0358	4,1.5,0.0033	5,1.5,0.0019
2_Co2	1	0.0	1,1.5,0.6610	2,1.5,0.2814	3,1.5,0.0542	4,1.5,0.0012	5,1.5,0.0006
	2	204.8	1,1.5,0.8664	2,1.5,0.0895	3,1.5,0.0361	4,1.5,0.0032	5,1.5,0.0020

Table S20. Calculated energy levels (cm^{-1}), g (g_x, g_y, g_z) tensors of the ground and first excited spin-orbit states of **2_Co1** and **2_Co2** using CASSCF/ RASSI-SO with MOLCAS 8.4.

	2_Co1		2_Co2	
	E/cm^{-1}	g	E/cm^{-1}	g
1	0.0	$g_x = 1.740, g_y = 2.114, g_z = 8.138$	0.0	$g_x = 1.743, g_y = 2.170, g_z = 8.091$
2	210.1	$g_x = 2.201, g_y = 2.939, g_z = 4.761$	204.8	$g_x = 2.228, g_y = 2.854, g_z = 4.871$

Table S21. Exchange energies E (cm^{-1}), the energy difference between each exchange doublets Δ_t (cm^{-1}) and the main values of the g_z for the lowest two exchange doublets of **1** and **2**. Energy is measured relative to the ground crystal field (m_j) state.

Exchange doublets in 1	E	Δ_t	g_z
1	0.00000000	0.396×10^{-5}	14.594
	0.00000396		
2	1.44777134	0.420×10^{-5}	36.725
	1.44777554		
Exchange doublets in 2	E	Δ_t	g_z
1	0.00000000	0.183×10^{-2}	32.207
	0.00000000		
2	2.00486577	0.196×10^{-1}	15.288
	2.00486577		
3	2.05528242	0.485×10^{-1}	17.687
	2.05528242		
4	3.85506596	0.315×10^{-2}	6.965
	3.85506596		

References:

- S1 Aquilante, F.; Autschbach, J.; Carlson, R. K.; Chibotaru, L. F.; Delcey, M. G.; De Vico, L.; Galván, I. F.; Ferré, N.; Frutos, L. M.; Gagliardi, L.; Garavelli, M.; Giussani, A.; Hoyer, C. E.; Li Manni, G.; Lischka, H.; Ma, D.; Malmqvist, P. Å.; Müller, T.; Nenov, A.; Olivucci, M.; Pedersen, T. B.; Peng, D.; Plasser, F.; Pritchard, B.; Reiher, M.; Rivalta, I.; Schapiro, I.; Segarra-Martí, J.; Stenrup, M.; Truhlar, D. G.; Ungur, L.; Valentini, A.; Vancoillie, S.; Veryazov, V.; Vysotskiy, V. P.; Weingart, O.; Zapata, F.; Lindh, R. *J. Comput. Chem.* **2016**, *37*, 506–541.
- S2 Chibotaru, L. F.; Ungur, L.; Soncini, A. *Angew. Chem., Int. Ed.* **2008**, *47*, 4126–4129.
- S3 Ungur, L.; Van den Heuvel, W.; Chibotaru, L. F. *New J. Chem.* **2009**, *33*, 1224–1230.
- S4 Chibotaru, L. F.; Ungur, L.; Aronica, C.; Elmoll, H.; Pilet, G.; Luneau, D. *J. Am. Chem. Soc.* **2008**, *130*, 12445–12455.
- S5 Lines, M. E. *J. Chem. Phys.* **1971**, *55*, 2977–2984.
- S6 Mondal, K. C.; Sundt, A.; Lan, Y. H.; Kostakis, G. E.; Waldmann, O.; Ungur, L.; Chibotaru, L. F.; Anson, C. E.; Powell, A. K. *Angew. Chem., Int. Ed.* **2012**, *51*, 7550–7554.
- S7 Langley, S. K.; Wielechowski, D. P.; Vieru, V.; Chilton, N. F.; Moubaraki, B.; Abrahams, B. F.; Chibotaru, L. F.; Murray, K. S. *Angew. Chem., Int. Ed.* **2013**, *52*, 12014–12019.